Unified analysis of global and focal aspects of absence epilepsy via neural field theory of the corticothalamic system

Dong-Ping Yang* and P. A. Robinson
School of Physics, University of Sydney, New South Wales 2006, Australia
and Center for Integrative Brain Function, University of Sydney, New South Wales 2006, Australia

(Received 22 May 2019; revised manuscript received 21 August 2019; published 10 September 2019)

Absence epilepsy is characterized by a sudden paroxysmal loss of consciousness accompanied by oscillatory activity propagating over many brain areas. Although primary generalized absence seizures are supported by the global corticothalamic system, converging experimental evidence supports a focal theory of absence epilepsy. Here a physiology-based corticothalamic model is investigated with spatial heterogeneity due to focal epilepsy to unify global and focal aspects of absence epilepsy. Numeric and analytic calculations are employed to investigate the emergent spatiotemporal dynamics as well as their underlying dynamical mechanisms. They can be categorized into three scenarios: suppressed epilepsy, focal seizures, or generalized seizures, as summarized from a phase diagram vs focal width and characteristic axon range. The corresponding temporal frequencies and spatial extents of cortical waves in generalized seizures and focal seizures agree well with experimental observations of global and focal aspects of absence epilepsy, respectively. The emergence of the spatiotemporal dynamics corresponding to focal seizures provides a biophysical explanation of the temporally higher frequency but spatially more localized cortical waves observed in genetic rat models that display characteristics of human absence epilepsy. Predictions are also presented for further experimental test.

DOI: 10.1103/PhysRevE.100.032405

I. INTRODUCTION

Absence epilepsy is an idiopathic nonconvulsive generalized epilepsy that displays a sudden paroxysmal loss of consciousness accompanied by abnormal brain oscillatory activity: 2.5- to 4-Hz "spike-and-wave" discharges (SWDs) in electroencephalogram (EEG), electrocorticogram (ECoG), and local field potentials (LFPs) [1–3]. These oscillations propagate rapidly over many brain areas and reflect macroscopic dynamical properties of neuronal populations. Many experimental results led to the corticothalamic theory that interactions between cortex and thalamus generate absence seizures [3–8]. However, converging evidence of animal "models" that display SWDs similar to those of absence epilepsy in humans [9–13] has shown that absence seizures can be triggered from a specific cortical focus, leading to a focal theory of absence epilepsy [2]. Also, an accurate source analysis from dense-array surface electrodes suggested that absence seizures in human patients were not truly "generalized," with immediate and global cortical involvement, but rather were initiated in specific cortical regions and then propagated to the whole cortex within milliseconds [14,15]. There remains a hot debate over the global and focal aspects of absence epilepsy [8,16–20].

So it is essential to study spatiotemporal dynamics of brain activities, exploring the conditions for focal epilepsy to be suppressed, to remain spatially localized, or to generalize and spread over the whole brain. However, spatial interactions involve complicated connectivity between cortical areas as well as subcortical structures, such as the thalamus [21–24], which can be responsible for various spatiotemporal patterns of large-scale brain activity [25]. In the mean-field theory, many neurons are averaged to get equations for mean membrane potential V and neuronal firing rate Q, and spatial couplings can be described by integrating the Green function or, in many cases, approximated by a corresponding differential form, most often a Laplacian [26–29]. Such mean-field theory has been successfully used to account for various macroscopic brain activities as measured through the electromagnetic signals (EEG and MEG), for normal states as well as generalized seizures [28–31]. However, it has not yet been explored whether the mean-field theory can provide a framework to unify both global and focal aspects of absence epilepsy, whether it can be used to explain the evolution from focal epilepsy to generalized seizures, and what is the underlying dynamical mechanism. Specifically, here we explore the role of the characteristic corticocortical axon range in the interactions between normal states and focal absence epilepsy.

The brain is a multiscale dynamical system in respect of both complicated structure and activity. The cellular mechanisms for generating SWDs were thoroughly studied in rodents [16,32,33], especially two genetic strains of rats: the Wistar Albino Glaxo/Rijswijk (WAG/Rij) and Genetic Absence Epilepsy Rats from Strasbourg (GAERS), which display similarities of simultaneous electroclinical signs and performance predictions based on behavioral and pharmacological data [32,34,35] from humans and are thus regarded as well established models, i.e., analogs of absence epilepsy in humans. One of the main differences is the higher frequency of SWDs: 7–11 Hz in rats [9,11] and 2.5–4 Hz in cats, rhesus monkeys, or humans [1,8,17]. The frequencies of SWDs have

*dp.yang@sydney.edu.au

been proposed to be accounted for based on the properties of $GABA_B$ receptors and T-type Ca^{2+}-channel- (T-channel) dependent burst firing in thalamocortical relay neurons [5]. The faster oscillations in rodents were also explained by involving $GABA_A$ conductance with fast dynamics in that population [36]. However, the origin of the slow timescale resulting from $GABA_B$ receptor activation has been challenged [33], and a recent thorough experiment study of behaviors in pathological rodents [20] has shown direct evidence against the viewpoint that $GABA_B$ receptors and T-channel-dependent burst firing in thalamocortical relay neurons are critical for absence seizures [5,37]. So it is still unknown what is the origin of higher rhythms of seizure activities in rodents, although there is no *a priori* reason for the same SWD frequency in all species. Here we propose network effects on the different frequencies, which may also involve interplay with cellular mechanisms.

On the other hand, the *spatial extent* of absence seizure activity is another significant difference between rats and other species, with SWDs in WAG/Rij rats more spatially localized than seizure activity in humans, which spreads widely over the whole cortex [8,14]. In these rats, spontaneous absence seizures are generated in a cortical "focus," which drives widespread corticothalamic networks, so that SWDs are intense in the cortical focus of the anterior cortex and corresponding thalamic nuclei, and decrease along the propagation direction on the cortex [9], until activity is very nearly normal in the occipital cortex, thalamic visual relay nuclei, hippocampus, and limbic thalamus nuclei, as demonstrated in the simultaneous electrophysiological recordings (LFPs, ECoGs, or EEG with simultaneous fMRI) [2,16,38]. It is also commonly found in experiments that lower-frequency resonances are much more generalized in space, than higher-frequency oscillations which are more localized to restricted cortical areas [39,40]. So it is essential to investigate whether and how spatial extents of seizure activities can account for the observed oscillations with different frequencies.

To this end, the spatiotemporal dynamics of the coupled cortex and thalamus are theoretically investigated using a physiology-based corticothalamic model with focal spatial heterogeneity, exploring the roles of cortical propagation and the spatial extent of focal epilepsy. We first introduce the corticothalamic model, numeric simulations, and analytic methods and then present the phase diagram of the spatiotemporal dynamics vs focal width and characteristic axon range. Specifically, the focal epilepsy with a relatively small width can be suppressed, one with a relatively large width can be generalized over the whole system with ∼3-Hz traveling waves, and one with a moderate width is limited to the focal region without generalizing into normal regions but with a ∼10-Hz rhythm. Their spatiotemporal properties such as spatial extents and temporal frequencies are comparable with experimental observations in humans and rats. The resulting cortical waves have robust frequencies, and their underlying dynamical mechanisms are discovered by employing eigenvalue spectra and corresponding eigenmodes of the critical states. Such emergence of the spatiotemporal dynamics corresponding to focal seizures provides a biophysical explanation of the temporally higher frequency, but spatially more localized, cortical waves observed in genetic rats. Thus we uncover a unified dynamical mechanism for the global and focal aspects of absence epilepsy, and conclude with experimentally testable predictions and further extensions for future work.

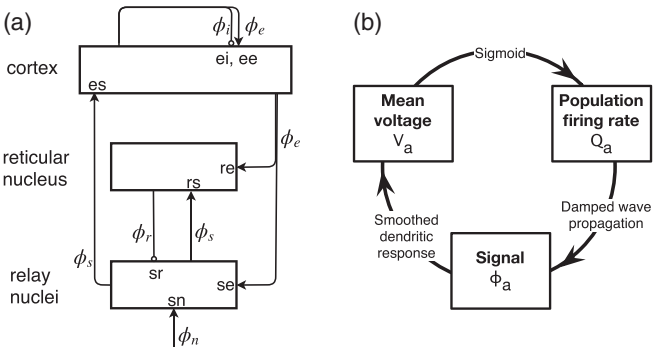

FIG. 1. The corticothalamic model. (a) Schematic of the corticothalamic interactions, showing the locations *ab* at which couplings act. Connectivity and loops include intracortical (*ee*, *ei*, *ie*, *ii*), corticothalamic (*re*, *se*), thalamocortical (*es*, *is*), and intrathalamic (*sr*, *rs*), as well as the ascending input from brainstem *sn*. (a) The physical interrelationship of the system variables: V_a, Q_a, and ϕ_a.

II. MATERIALS AND METHODS

Our corticothalamic model is described following previous work [30,31] and specified here with spatial heterogeneity due to focal epilepsy. Then, we describe simulation methods, analytic calculations of steady states, and their linear stability analysis.

A. Corticothalamic model

The corticothalamic system can be described by a continuum approach at the macroscopic level, where large-scale neural activities are determined by interactions between several neural populations, notably excitatory and inhibitory cortical neurons and thalamus, including reticular and relay nuclei. A schematic of these populations is presented in Fig. 1(a), with excitatory, inhibitory, reticular, and relay neurons represented by e, i, r, and s, respectively. Figure 1(b) summarizes the physical interrelationship of the collective state variables, which are the local mean values at position $\boldsymbol{r} = (r_x, r_y)$ in a two-dimensional (2D) space: the local mean cell-body potential V_a, the mean firing rate Q_a, and the propagating axon field ϕ_a, for $a = e, i, r, s$ [30]. The spatially distributed corticothalamic model is illustrated in Fig. 2. The spatial position $\boldsymbol{r} = (r_x, r_y)$ is assigned to both the cortex and the thalamus, and the thalamus has a one-to-one map to the cortex. The cortex is modelled as a square sheet with a side length L, while the thalamus is modelled as a 2D sheet with a tenth scaled side length $L/10$. Here we unify human ($L = 0.5$ m) and rat ($L = 0.025$ m) brains into a unique framework here, with assumption of linear proportionality of other spatial properties in these two systems.

First, the firing rate Q_a is a sigmoid function of the potential V_a, with

$$Q_a(\boldsymbol{r}, t) = S[V_a(\boldsymbol{r}, t)] = \frac{Q_{\max}}{1 + \exp[\theta - V_a(\boldsymbol{r}, t)]/\sigma'}, \quad (1)$$

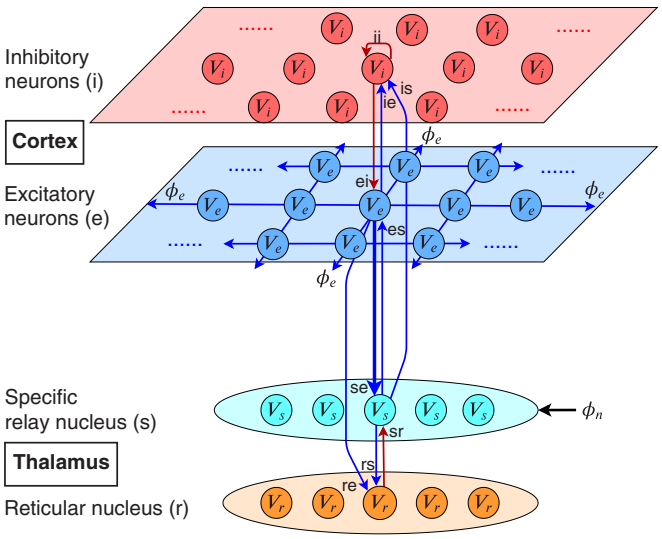

FIG. 2. Illustration of the spatially distributed corticothalamic model. The cortex is modelled as a 2D sheet with a side length L and the thalamus is 10th rescaled with a side length $L/10$ ($L = 0.5$ m for human brains and $L = 0.025$ m for rat brains). Each spatial point $\boldsymbol{r}$ describes local mean-field dynamics of populations of excitatory and inhibitory neurons, interacting with neurons in the spatially corresponding specific relay and reticular nuclei of the thalamus. *ee* represents the cortical wave propagation of ϕ_e as described in Eqs. (2) and (3). Arrows indicate excitatory feedback (blue) and inhibitory feedback (red). *se* is thickened to indicate that ν_{se} is strengthened to model focal absence seizure, as discussed in detail in Sec. II B.

where $Q_{\max}$ is the maximal firing rate, θ is the mean firing threshold, and $\sigma'\pi/\sqrt{3}$ is the standard deviation of the difference between the steady state V_a and the threshold θ.

Second, neuronal firing generates a field signal ϕ_a and sends it through the extended axons toward other populations, approximately according to the damped wave equation [27,28]

$$\left(D_a - r_a^2\nabla^2\right)\phi_a(\boldsymbol{r},t) = Q_a(\boldsymbol{r},t), \tag{2}$$

with

$$D_a = \left(\frac{1}{\gamma_a}\frac{\partial}{\partial t} + 1\right)^2, \tag{3}$$

where $\gamma_a = v_a/r_a$ governs the damping of propagating waves, and r_a and v_a are the characteristic range and conduction velocity of the axons of population a, respectively [28]. The Laplacian in Eq. (2) is the differential form of a spatially extended kernel that incorporates axon ranges with an approximately exponential distribution with a characteristic range r_a [28]. The differential and integral forms are exactly equivalent.

Finally, each population's potential V_a results when synaptic inputs from various types of afferent neurons are summed after being filtered and smeared out in time due to synaptic neurotransmitter, receptor dynamics, passage through a dendritic tree and effects of soma capacitance. So we have

$$D_\alpha V_e(\boldsymbol{r},t) = \nu_{ee}\phi_e(\boldsymbol{r},t) + \nu_{ei}\phi_i(\boldsymbol{r},t) + \nu_{es}\phi_s(\boldsymbol{r},t-t_d), \tag{4}$$

$$D_\alpha V_r(\boldsymbol{r},t) = \nu_{re}\phi_e(\boldsymbol{r},t-t_d) + \nu_{rs}\phi_s(\boldsymbol{r},t), \tag{5}$$

$$D_\alpha V_s(\boldsymbol{r},t) = \nu_{se}\phi_e(\boldsymbol{r},t-t_d) + \nu_{sr}\phi_r(\boldsymbol{r},t) + \nu_{sn}\phi_n(\boldsymbol{r},t), \tag{6}$$

TABLE I. Nominal parameter values in spatially homogeneous model from Refs. [31,44].

Parameter	Value	Unit	Parameter	Value	Unit
$Q_{\max}$	250	s^{-1}	ν_{ee}	1.0	mV s
θ	15	mV	$-\nu_{ei}$	1.8	mV s
σ'	6	mV	ν_{es}	3.2	mV s
α	50	s^{-1}	$-\nu_{sr}$	0.8	mV s
β	200	s^{-1}	$\nu_{sn}\phi_n$	2.0	mV s
γ_e	100	s^{-1}	ν_{re}	1.6	mV s
t_d	40	ms	ν_{rs}	0.6	mV s
			$\nu_{se}(\boldsymbol{r})$	1.8∼4.4	mV s

with the synaptodendritic operator

$$D_\alpha = \frac{1}{\alpha\beta}\frac{d^2}{dt^2} + \left(\frac{1}{\alpha}+\frac{1}{\beta}\right)\frac{d}{dt} + 1, \tag{7}$$

where α and β are the mean decay and rise rates of the soma response to an impulse arriving at a dendritic synapse [28]. Notice that the dynamics of inhibitory population is retained, but is not explicitly expressed in Eqs. (2)–(7), because intracortical connectivities have been found to be proportional to the numbers of synapses involved [41,42], so one has $V_e = V_i$ and $Q_e = Q_i$ [30,43], which allows us to concentrate on excitatory quantities, while implicitly retaining inhibitory effects on the dynamics. Besides, all populations except the excitatory population have very short axons, which lets us set $r_a \approx 0$ and $\gamma_a \approx \infty$ in (3), yielding $\phi_a = Q_a$ for $a = i, r, s$ [30]. Input from the thalamus to the cortex and feedback from the cortex to the thalamus are delayed by a propagation time t_d. In Eqs. (4)–(6), ν_{ab} is the synaptic connection strength to population a from population b, and ϕ_n is the ascending input from brainstem, which can be arbitrary external signals or approximated as white noise, but here is set to a constant for calculating phase diagrams and bifurcation diagrams.

Thus, the model includes 16 parameters: $Q_{\max}$, θ, σ', α, β, γ_e, t_d, r_e, ν_{ee}, ν_{ei}, ν_{es}, ν_{se}, ν_{sr}, $\nu_{sn}\phi_n$, ν_{re}, ν_{rs}, which are enough to allow realistic representation of the most salient anatomy and physiology, but few enough to yield useful interpretations. Their values are presented in Table I.

B. Model of focal spatial heterogeneity

In WAG/Rij rats with absence seizures, the SWDs are initiated from the deep layer neurons of the cortical focus–the facial somatosensory cortex, due to imbalance of excitation and inhibition therein [11,32,34]. It has been investigated that the excitatory dendrites in the focal region have larger total dendrite length, larger mean length of a dendritic segment, and larger size of dendritic arbor, than those outside epileptic area [17,34]. Additionally, the excitatory-inhibitory ratio of neuron numbers in focal cortical areas is larger than that in other areas and the efficiency of GABA-ergic inhibition is impaired [34].

Later, the SWDs can be sustained and then propagate via regional and distant layer five axonal projections within the somatosensory cortex and to other cortical and thalamic regions, where corticothalamic and thalamocortical neurons drive each other forming a unified oscillatory system. Lesion studies also demonstrate that an excitable region is not

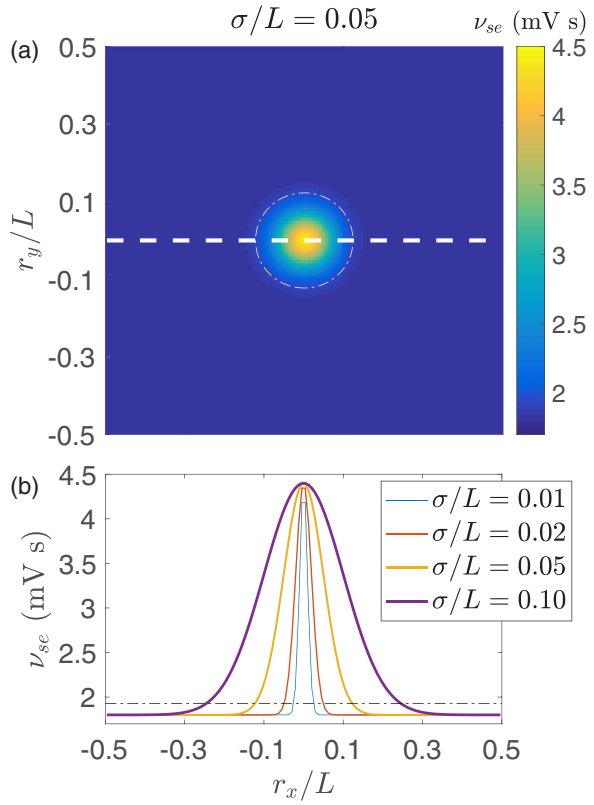

FIG. 3. Spatially heterogeneous corticothalamic model. (a) Schematic of the 2D spatial model with periodic boundary conditions; Each position $\boldsymbol{r} = (r_x, r_y)$ represents a corticothalamic loop with $\nu_{se}(\boldsymbol{r})$ determined by a spatially Gaussian profile given in Eq. (8) with $\sigma/L = 0.05$, $\nu_{se}(L/2) = 1.8$ mV s, and $\nu_{se}(0) = 4.4$ mV s. The white dashed line indicates the position of the spatial profiles in (b). (b) Spatially Gaussian profiles $\nu_{se}(\boldsymbol{r})$ along r_x at $r_y = 0$ with various σ/L, as indicated in the legend. The white dash-dotted circle in (a) and the black dash-dotted line in (b) indicate the threshold ν_{se}^c for transition to absence seizures in the spatially homogeneous case. They are also used to define the region inside for focal epilepsy and the normal region outside.

sufficient for the occurrence of SWDs and indicate that some thalamic nuclei seem to be important for SWD occurrence [7], as implied by theory and simulations [30,31].

Although the excitation-inhibition imbalance in the focus is essential for SWDs initiation, the key for sustaining the SWDs lies in the interaction between cortex and thalamus. Thus, here we model the focus with a higher value of ν_{se}, which describes the excitatory influence of cortical pyramidal cells on the specific thalamic nuclei, due to the hyperactivity of excitatory neurons in the focus, emphasizing the interaction between cortex and thalamus. In the model, a higher value of ν_{se} in the focal area is set to describe focal epilepsy, with ν_{se} peaking at the center and smoothly decreasing to the edge, as shown in Fig. 3(a). The choice of ν_{se} is also supported by prior implications of excitatory corticothalamic feedback in the pathophysiology of generalized absence seizures [9,32,38,45]. As studied in our previous work [30,31,44], especially in the normal form analysis of Hopf bifurcations dependent on both ν_{se} and ν_{es} [44], ν_{es} should have similar effects on the system stability and induction of absence seizures.

Thus, the corticothalamic model with focal spatial heterogeneity is employed to investigate the effect of cortical propagation on the spatiotemporal dynamics, and to study how focal epilepsy can be suppressed, remain localized, or propagate over the whole brain to produce secondary generalized absence seizures.

For simplicity, the spatial profile is set to be an isotropically symmetric Gaussian function

$$\nu_{se}(\boldsymbol{r}) = [\nu_{se}(0) - \nu_{se}(L/2)] \exp(-|\boldsymbol{r}|^2/2\sigma^2) + \nu_{se}(L/2), \tag{8}$$

with σ characterizing the pathological width, $\nu_{se}(L/2)$ the background normal value and $\nu_{se}(0)$ the pathological value. Figure 3(b) shows profiles along r_x/L at $r_y = 0$ with various σ/L. All other parameters are spatially invariant, as given in Table I.

The isotropic symmetry is limited by boundary, which has little effect on the symmetry if we choose $\sigma/L \ll 1$ and $r_e/L \ll 1$ but still brings edge effects on the spatiotemporal dynamics, as we demonstrate in Sec. III.

C. Simulation methods

The model is simulated using the recently published NFTsim code written in C++ [46] to investigate the spatiotemporal dynamics [30,31,44], which solves our damped and retarded 2D wave equation in Eqs. (2) and (4)–(6) with given initial conditions and boundary conditions.

In numerical simulations, the 2D space (r_x, r_y) is divided into a 120×120 grid with $L = 0.5$ m for humans and $L = 0.025$ m for rats, and grid point spacing $\delta r_x/L = \delta r_y/L = 1/120$. We choose periodic boundary conditions and an initial condition that each spatial point is assigned with a τ_d length time series of a random constant.

In NFTsim, numerical integration is performed using a fourth-order Runge-Kutta integrator. A cubic-spline interpolator is employed in order to estimate the time-delayed values of the midpoints required for the Runge-Kutta algorithm. A small time step ($\delta t = 0.1$ ms) is chosen to satisfy the Courant condition [47], that is, the *Courant number* $C = \frac{u_x \delta t}{\delta r_x} + \frac{u_y \delta t}{\delta r_y} \leqslant 1$, where u_x and u_y are the magnitudes of the velocity [46]. Long (~1000 s) simulations, which cost ~10 h of real time on the cluster with Intel Xeon CPU 2.10 GHz, are performed to guarantee the system reaches its stationary state.

Noise is ignored in the simulations for phase diagrams and bifurcation diagrams, to simplify our analysis so as to focus on pattern formation and its underlying dynamical mechanism. We have checked that weak noise has no significant effect on our findings, but strong noise can destroy pattern formation, as demonstrated in Sec. III C.

D. Steady states and linear stability analysis

To get more insight of underlying mechanisms for various spatiotemporal dynamics, we are introducing here analytic methods how to derive the steady states, their linear stability and eigenmodes.

As introduced above, the system has a radial symmetry with $\sigma/L \ll 1$ and $r_e/L \ll 1$, leading to the replacement of $\boldsymbol{r}$ by $r = |\boldsymbol{r}|$ to simplify our analysis. Then the spatial interaction in radial coordinates can be rewritten as

$$\mathscr{L} \triangleq r_e^2\nabla^2 = r_e^2\left(\frac{\partial^2}{\partial r^2} + \frac{1}{r}\frac{\partial}{\partial r}\right). \tag{9}$$

As proposed in Ref. [48], the steady states can be obtained by integrating Eqs. (2), and (4)–(6) inward toward $r = 0$, starting at a large r, where the system can be linearized with r to be

$$\left[\mathscr{L} - L_{\mathrm{CT}}^{-1}(0, r)\right]\phi_e(r) = 0, \tag{10}$$

with the function $L_{\mathrm{CT}}^{-1}(\lambda, r)$ given by Eq. (A12) in Appendix A, which describes the resonance [at $L_{\mathrm{CT}}^{-1}(\lambda, r) = 0$] of the corticothalamic loop at r and the eigenmode with an eigenvalue λ. The stationary state converges asymptotically to the solution at large r, and the appropriate boundary condition at $r = 0$ is

$$\partial\phi_a(0)/\partial r = 0. \tag{11}$$

Thus one of its general solutions, converging at $r \to L/2 \gg r_e$, is

$$\phi_e(r) = BK_0\left[\frac{r}{r_e}\sqrt{L_{\mathrm{CT}}^{-1}(0, r)}\right] + \phi_e(L/2), \tag{12}$$

where K_0 is a modified Bessel function of the second kind and B is an undetermined real constant, which uniquely parametrizes the stationary solution to the nonlinear equations (2) and (4)–(6). So our task is to search for the value of B for which the solution $[\phi_e^0(r), V_e^0(r), V_r^0(r), V_s^0(r)]$ obeys the boundary condition (11).

To analyze linear stability of the steady state, a small dimensionless perturbation can be introduced as follows:

$$\chi_a(r, t) = \left[\phi_a(r, t) - \phi_a^0(r)\right]/Q_{\max}, \tag{13}$$

$$v_a(r, t) = \left[V_a(r, t) - V_a^0(r)\right]\eta_a(r)/\sigma', \tag{14}$$

$$q_a(r, t) = \left[Q_a(r, t) - Q_a^0(r)\right]/Q_{\max}, \tag{15}$$

with $\sigma' = \sigma\sqrt{3}/\pi$, $\eta_a(r) = q_a^0(r)[1 - q_a^0(r)]$, and $q_a^0(r) = Q_a^0(r)/Q_{\max}$ for $a = e, r, s$. The perturbations can be expanded in sums of eigenmodes as follows:

$$\chi_e(r, t) = \sum_i C_i \exp(\lambda_i t)\hat{\chi}_e(\lambda_i, r), \tag{16}$$

$$q_a(r, t) = \sum_i C_i \exp(\lambda_i t)\hat{q}_a(\lambda_i, r), \tag{17}$$

each of which obeys

$$\left[\mathscr{L} - L_{\mathrm{CT}}^{-1}(\lambda_i, r)\right]\hat{\chi}_e(\lambda_i, r) = 0, \tag{18}$$

$$\left[D(\lambda) - L_{\mathrm{CT}}^{-1}(\lambda_i, r)\right]\hat{\chi}_e(\lambda_i, r) = \hat{q}_a(\lambda_i, r), \tag{19}$$

with the function $D(\lambda)$ given by Eq. (A6) in Appendix A. Again, a unique bounded solution for $\hat{\chi}_e(\lambda_i, r)$ at $r \to L/2$ is

$$\hat{\chi}_e(\lambda_i, r) = K_0\left[\frac{r}{r_e}\sqrt{L_{\mathrm{CT}}^{-1}(\lambda_i, r)}\right]. \tag{20}$$

Note that there is no constant B as in the steady-state equation (12) because it has been absorbed into C_i. So now our task is to search for the eigenvalue λ_i as well as the corresponding perturbation eigenmode. The largest $\mathrm{Re}(\lambda_i)$ determines linear stability of the steady state.

III. SPATIOTEMPORAL DYNAMICS

The spatiotemporal dynamics are presented starting from the spatially homogeneous case. Then the corticothalamic system with focal epilepsy is investigated by numeric simulations to study how cortical propagation can suppress, localize, or generalize the focal epilepsy, and to explore various spatiotemporal dynamics. Traveling waves that emerge from the focus in various phases are investigated and compared with experimental observations in humans and rats, yielding predictions to be further tested experimentally.

A. The spatially homogeneous case

The corticothalamic system has been employed to understand and unify many features of normal EEGs, including discrete spectral peaks in slow-wave, delta, theta, alpha, and beta bands, observed in waking and sleeping states, and evoked response potentials [30,49]. The normal oscillations, i.e., ~3-Hz waves and ~10-Hz waves, were found to converge to linear, near-equilibrium dynamics at macroscopic scales [28,43,50,51], whereas pathological oscillations in generalized epilepsies were found to converge to nonlinear behaviors beyond linear stability with hypersynchrony in the neuronal populations and many nonlinear features of large-scale brain activities comparable with experimental real data [30,31,52]. So, the relevant linear stability of large-scale brain dynamics can be regarded as the criterion for separating normal activity from seizurelike oscillations.

Together, the cortex and the thalamus form a complex oscillatory network, providing a resonant circuit to amplify and sustain the SWDs, with the resonance being an emergent property of the corticothalamic system [3,53]. Specifically, bifurcations have been intensively investigated via changes of the parameter ν_{se}, and it has been demonstrated that this system can explain primary generalized absence seizures [30,31]. Furthermore, recent analysis has established a bridge that explicitly links the tractable normal-form dynamical parameters with the underlying physiological ones [44].

In the homogeneous case for generalized absence seizures, the system has spatially uniform activity and the corticothalamic loop experiences a supercritical Hopf bifurcation, then a period-doubling, when ν_{se} ranging from $\nu_{se}(L/2)$ to $\nu_{se}(0)$, as shown in the bifurcation diagram of Fig. 4(a). In Fig. 4(b), various dynamical states are evidenced by time series of ϕ_e at various ν_{se}, whose values are correspondingly indicated by the red dashed lines in Fig. 4(a). Specifically, one can find oscillating dynamics with a ~3-Hz rhythm and the stereotyped SWDs. The presented dynamics can be found over a wide range of parameters. This is one example. This result has been compared with clinical data in detail and thus was employed to explain the pathological transition from normal arousal states to primary generalized absence seizures [30,31].

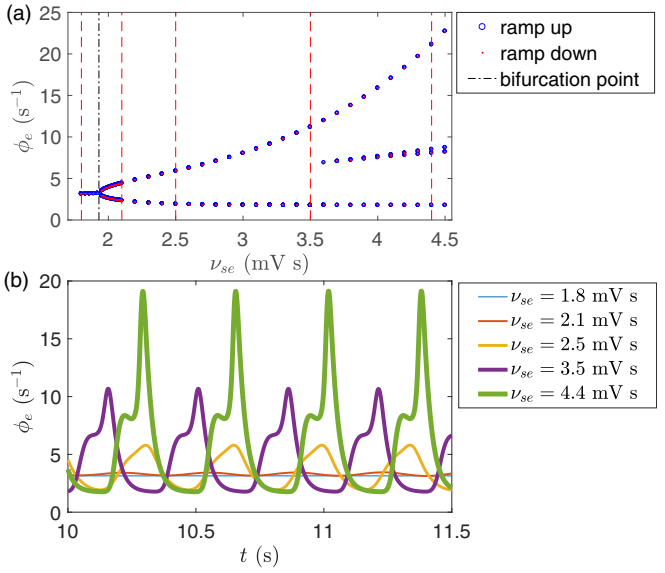

FIG. 4. Bifurcation in the spatially homogeneous case. (a) Bifurcation diagram of ϕ_e when ν_{se} ramps up and down from $\nu_{se}(L/2)$ to $\nu_{se}(0)$ and vice versa. The black dashed line indicates the threshold ν_{se}^c for Hopf bifurcation. (b) Time series of ϕ_e for various ν_{se} indicated by the red dashed lines in (a).

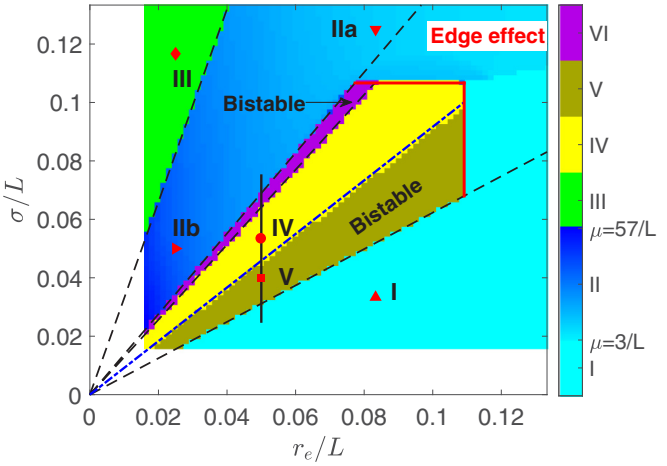

FIG. 5. Phase diagram of spatiotemporal dynamics vs axon range r_e and focal width σ both scaled by L showing six phases. The instability line for ∼10-Hz oscillation is predicted by linear stability analysis as indicated by the blue dash-dotted line, while other phase separations are indicated by the black dashed lines. Six examples are indicated by various shaped red points, with the corresponding spatiotemporal dynamics of ϕ_e shown in Fig. 6. The attenuation factor μ scaled by $1/L$ is also indicated in the colorbar for Phase II. Note that edge effects limit Phases IV, V, and VI. The black vertical line indicates the parameter range further investigated in Fig. 7.

B. From suppressed epilepsy to generalized seizures

Here we show that secondary generalized absence seizures can be induced by focal epilepsy. The induced absence seizures can have various spatial extents and oscillating frequencies, if we explore the roles of σ and r_e. Actually, both of them are constrained by the system size L, yielding edge effects. Thus, we investigate various spatiotemporal dynamics vs r_e/L and σ/L with $r_e/L \ll 1$ and $\sigma/L \ll 1$, summarized in the phase diagram as shown in Fig. 5, which has six different phases, with Phases I, II, and III discussed in this subsection, and Phases IV, V, and VI in the next.

Notice that numeric simulations in the left and bottom white bands of Fig. 5 would require impractically long simulation time. In those regions, the default grid spacing would need to be reduced to smaller δr_x and δr_y, resulting in smaller time step δt via the Courant condition [47]. For example, halving δr_x and δr_y will halve δt, resulting in 8 fold of the total simulation time.

In Phase I, focal epilepsy with small σ is suppressed by axonal projections from the normal region if r_e is large as in the case of healthy adults [54]. The activity profile of suppressed epilepsy stabilizes with slightly enhanced, but temporally constant, activity in the center, as shown in Fig. 6(a).

In Phase II, the focal epilepsy with large-enough σ can resist suppression, and even propagate and destabilize the whole system, leading to secondary generalized absence seizures, which originate from a ∼3-Hz oscillating focus and propagate rapidly outward to the whole system, but with the wave amplitude attenuated along r, as shown in Figs. 6(b) and 6(c). The attenuation can be characterized by an attenuation factor $\mu = \partial \log \phi_e(r)/\partial r$, as indicated in Fig. 5, with larger μ at smaller r_e. Here μ is scaled by $1/L$, with its value characterizing the times of attenuated ϕ_e amplitude when the wave travels through the system. The phase velocity is discussed below in Sec. III D. Here the system transits continuously from suppressed epilepsy in Phase I to generalized seizures in Phase II via a supercritical Hopf bifurcation with the oscillation amplitude of $\phi_e(0)$ increasing gradually from zero, as indicated in the upper right corner of Fig. 5; This transition is due to the boundary induced edge effects.

In Phase III, the direction of propagating waves is reversed from outward in Phase II to inward if r_e is small enough, as shown in Fig. 6(d), where the propagation direction is denoted by a red arrow. In future, wave-front instability analysis could be employed to understand this reversal [55].

C. Spatially limited focal seizures

In Phase IV, the focal epilepsy can be spatially limited to the focal region, with cortical activity decaying rapidly in the normal region, as demonstrated in the upper panel of Fig. 6(e), rather than spreading over the whole system as shown in Figs. 6(b)–6(d). More interestingly, the temporal rhythm is not ∼3 Hz any more, but induced by the spatiotemporal interactions to have a higher temporal frequency of ∼10 Hz.

The ∼10-Hz wave is not only spatially localized but also temporally modulated at ∼2 Hz, as shown in Fig. 6(e), which is reminiscent of complex-partial seizures with impaired consciousness [56,57]. The complex-partial seizures have stronger 1- to 2-Hz delta-range modulation in the bilateral frontal and parietal neocortex than simple-partial seizures, where consciousness is not impaired [56,57]. Thus the temporally modulated, spatially localized ∼10-Hz activity is a potential mechanism for the generation of complex-partial seizures, although we do not consider this point further here.

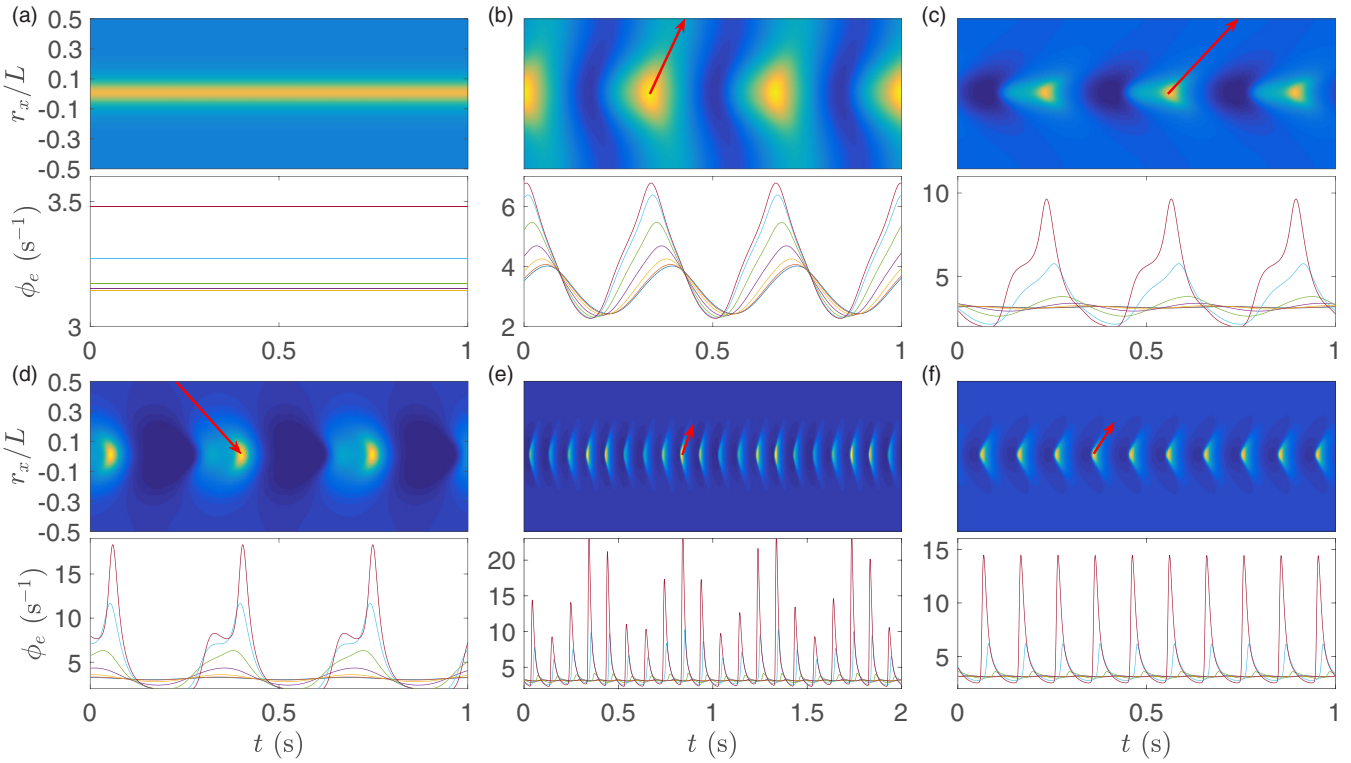

FIG. 6. Examples of various waves with parameter values of $(r_e/L, \sigma/L)$ indicated by the corresponding shaped red points in Fig. 5. All dynamics are radially symmetrical, so only 1D wave dynamics is presented. In each case, the upper panel presents the 1D wave dynamics of points at $r_y = 0$, indicated by the white dashed line in Fig. 3(a), while the lower panel shows the corresponding time series at seven equally spaced points from center to edge with decreasing ϕ_e [for (a)] or its amplitude [for (b)–(f)]. The values ϕ_e in upper panels from dark blue to yellow range from the minimal to the maximal ϕ_e in the corresponding lower panels. (a) Phase I, epilepsy suppressed. (b) Phase IIa, the wave weakly attenuated along $\boldsymbol{r}$. (c) Phase IIb, the wave strongly attenuated along $\boldsymbol{r}$. (d) Phase III, the wave propagating inward from edge to the center. (e) Phase IV, the spatially limited ∼10-Hz wave modulated by a ∼2-Hz slow wave. (F) One state in Phase V: the spatially limited regular ∼10-Hz wave, which coexists with the suppressed epilepsy. Wave propagation is indicated by red arrows in (b)–(f), whose slopes are the phase velocities.

The above modulation implies existence of spatiotemporal nonlinear wave interactions. Thus, in Fig. 7, we investigate the bifurcation diagram for the steady state of $\phi_e(0)$ against σ/L at $(r_x, r_y) = (0, 0)$. It shows that the system experiences a subcritical Hopf bifurcation from a fixed point to a limit cycle, and then a second Hopf bifurcation to a quasiperiodic cycle, e.g., a 2-torus, then a 3-torus, then higher-dimensional dynamics, and finally a chaotic attractor. Such a route to a chaotic attractor is induced by the nonlinear wave interactions, which can also terminate the chaotic dynamics and produce secondary generalized absence seizures when σ/L is large enough, as shown at the right end of the bifurcation diagram in Fig. 7. It is different from that observed previously in the homogeneous case, which is induced by the nonlinear corticothalamic interaction loop [44].

In Phase V, the system has two stable states: suppressed epilepsy and localized ∼10-Hz waves. In comparison with Phase IV, Phase V has a smaller σ/L and weaker nonlinear wave interactions. As a result, the localized ∼10-Hz wave in Phase V is regular without low frequency modulation, as demonstrated in Fig. 6(f). Actually, this bistability emerges from the subcritical Hopf bifurcation with hysteresis, and the system experiences a sudden transition from suppressed epilepsy to focal seizures at the critical point indicated by the green dashed line in Fig. 7. The instability boundary is consistent with the linear stability analysis as introduced under *Methods*. This subcritical Hopf bifurcation provides a new route for the transition from normal arousal states to epileptic seizures [6,52].

In Phase VI, the system has another two stable states: suppressed epilepsy and generalized seizures. In comparison with Phase IV, Phase VI has a larger σ/L and then stronger nonlinear wave interactions, which can terminate the spatially chaotic dynamics and turn the system into the second generalized seizures. This bistable region has just a narrow parameter range and may be hard to observe in experiments.

In the previous studies of neural fields [58,59], such localized ∼10-Hz waves in Phases IV, V, and VI are called as breathers. They emerge when the suppressed epilepsy becomes unstable and the instability boundary can be well predicted by linear stability analysis, as indicated by the blue dash-dotted line in Fig. 5. All other phase boundaries are also fully determined by the rescaled focal width $\hat{\sigma} = \sigma/r_e$ (the dashed lines in Fig. 5). Nonetheless, they terminate at large σ/L and r_e/L due to edge effects in the upper right corner of Fig. 5. Such spatially limited focal seizures emerge in the system with large-enough length to avoid edge effects, indicating that such phenomenon can exist in general

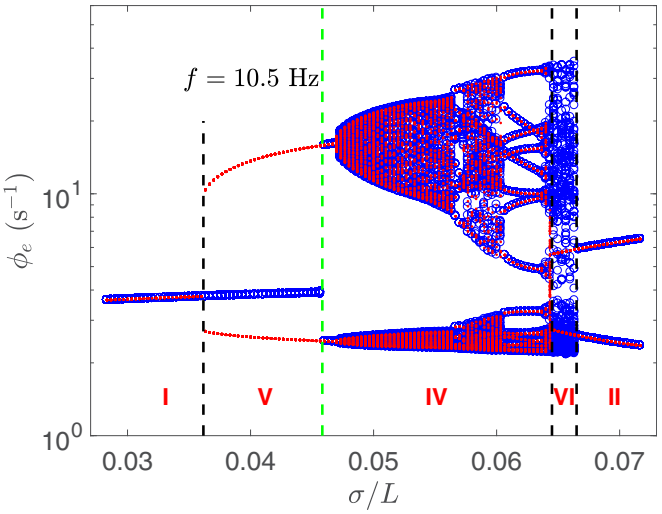

FIG. 7. Bifurcation diagram of $\phi_e(0)$ against σ/L, with two bistable regions, corresponding to Phase V and VI, respectively. The critical point for bifurcation from suppressed epilepsy to the focal seizures with a frequency $f = 10.5$ Hz is consistent with linear stability analysis, as indicated by the green dashed line. Blue circles, ramp up; red dots, ramp down; $r_e/L = 0.05$.

boundary conditions and cortical geometries; e.g., spherical topology brain hemisphere. Thus, our results hold for general scenarios with various spatial scales; e.g., various axon ranges r_e/L, whenever there is no edge effect, and they can also be applied in a scenario with multiple epilepsy foci, which spread widely in space and have weak mutual interactions.

Moreover, as demonstrated in Fig. 8, such localized waves in the above phases are stable in the presence of weak noise in the system, but can be disrupted by strong noise to yield generalized ∼3-Hz traveling waves similar to those in Phase II. Notice that the localized spatiotemporal patterns with different σ/L can resist different noise levels. The resistance is not monotonically dependent on σ/L as demonstrated in Fig. 8.

D. Traveling-wave properties

The propagating waves of electrical activity in the cortex have been observed during seizures in rats, cats, monkeys, and humans, with wave velocities of 0.01 to 10 m s^{-1}, depending on the cortical states and data analysis methods [60–67]. Here we consider the phase velocity v_p, defined over the whole system for the generalized seizures, while for the focal seizures, the wave does not propagate over the whole system and we define its effective region to be where oscillating amplitudes are larger than 0.03 times the maximum.

As shown in Fig. 9, for the generalized seizures, ∼3-Hz activity propagates over the whole system at the phase velocity $v_p/L = 20$ to 300 s^{-1}, while for the focal seizures, ∼10-Hz activity spreads only within the effective region at $v_p/L =$ 22 to 60 s^{-1}, which is significantly larger than the axon propagation speed, which can be estimated to be $v_e/L \approx r_e\gamma_e/L \leqslant 13$ s^{-1}. In the focal seizures, v_p/L depends linearly on the width w/L of the effective region with $0.3 < w/L < 0.8$, as shown in Fig. 9(a). Figures 9(b) and 9(c) show that v_p

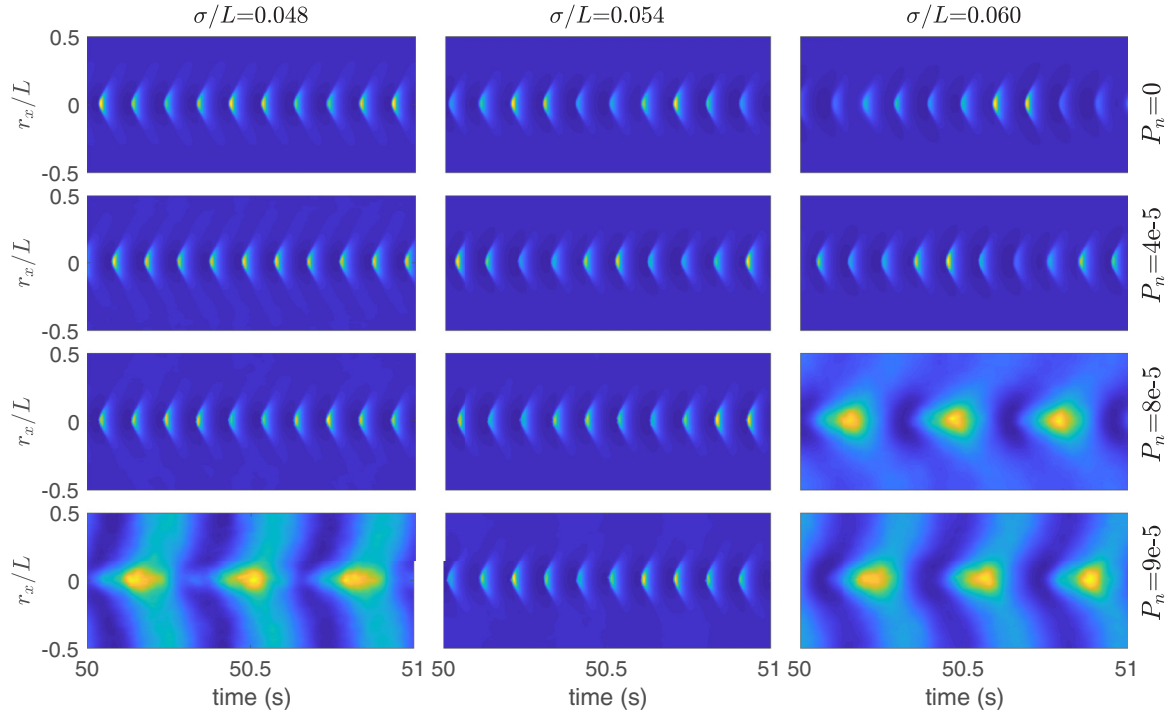

FIG. 8. Effect of noise on the observed localized spatiotemporal pattern with various normalized pathological widths σ/L (its value for each column is indicated on the top) and noise levels (its power density P_n for each row as indicated at the right) in the simulations of $r_e/L = 0.05$. The spatially localized ∼10-Hz wave can stay for the presence of a weak noise in the system, but can be broken by a strong noise into a generalized ∼3-Hz traveling wave similar to that in Phase II.

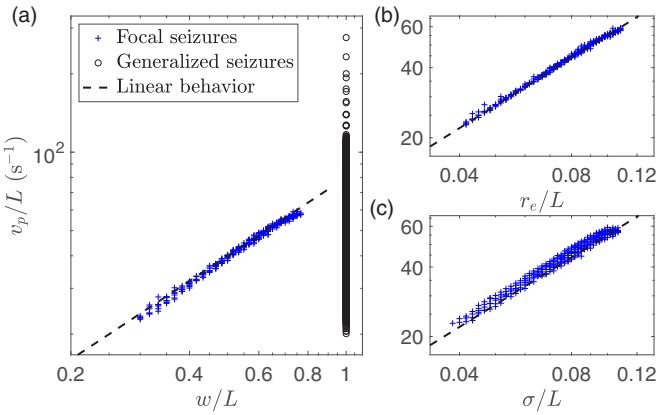

FIG. 9. Phase velocity v_p of the traveling waves. The points represent the cases with various parameter pairs $(r_e/L,\ \sigma/L)$ in Phases II and IV with $r_e/L \geqslant 0.05$. (a) v_p/L vs w/L in Phase II (open circle) and Phase IV (plus). (b) v_p/L vs r_e in Phase IV. (c) v_p/L vs σ in Phase IV. Linear proportionality is indicated by the dashed lines with slope 1 in the log-log plots.

also depends linearly on σ and r_e, to be

$$v_p/L = c + a_1 r_e/L + a_2 \sigma/L, \tag{21}$$

with $c = 0.80 \pm 0.17\ \mathrm{s}^{-1}$, $a_1 = 440 \pm 21\ \mathrm{s}^{-1}$ and $a_2 = 107 \pm 18\ \mathrm{s}^{-1}$. These predictions are potentially testable in experiments.

The linear dependence is consistent with the robust frequencies of the localized ∼10-Hz waves, which is independent of r_e/L or σ/L. As shown in the upper panel of Figs. 6(e) and 6(f) as well as in their eigenmodes to be discussed in the next subsection, the wave has only one peak vs r at each time, yielding the wave number $k \propto 1/w$, and then a constant frequency $f = v_p k/2\pi$.

IV. UNDERLYING DYNAMICAL MECHANISMS

From the above, our corticothalamic model with focal spatial heterogeneity can produce secondary generalized absence seizures with ∼3-Hz traveling waves which spread over the whole system (Phase II), and spatially more localized ∼10-Hz waves (Phase IV) as observed in the electrophysiological recordings (LFPs, ECoGs, or EEG) of WAG/Rij rats [9]. The spatiotemporal properties in Phase II and Phase IV, such as spatial extents and temporal frequencies, are comparable with experimental observations in humans and rats, respectively. The resulting cortical waves have robust frequencies in each phase. Therefore, the spatiotemporal dynamics in these two phases can account for the global and focal aspects of absence epilepsy, respectively, leading to the unification of these aspects into our corticothalamic model.

In the following, we also uncover underlying dynamical mechanisms for various phases, using eigenvalue spectra and corresponding eigenmodes at critical states. Then the role of the corticothalamic loop, especially the effects of the time lag t_d between cortex and thalamus, is investigated. Finally, we show robustness of the dynamical mechanisms.

A. Dynamical mechanism of spatially localized seizures

In our previous work of the homogeneous corticothalamic system [30,31,44], ∼3-Hz waves and ∼10-Hz waves were generated due to resonances in two different delayed feedback loops: $e \to r \to s \to e$ and $e \to s \to e$, respectively. But here a spatially localized ∼10-Hz wave emerges from focal epilepsy that has an intrinsic ∼3-Hz rhythm. So, it is not clear whether the localized ∼10-Hz wave originates from the same resonance of the underlying corticothalamic loop as in the homogeneous system, or is induced by the focal epilepsy via a different dynamical mechanism.

To this end, we investigate the steady states and corresponding eigenvalue spectra of the induced waves, as summarized in Fig. 10, where (a) and (b) show the three eigenvalues λ with the largest Re(λ) vs σ/L: the blue curve corresponds to the focal seizures with $f = 10.5$ Hz and the red ones to the generalized seizures with $f = 3.1$ Hz. The largest Re(λ) determines linear stability of the system, negative for the system to be stable and positive to be unstable.

Now we focus on the following three typical scenarios: (i) Phase I: suppressed epilepsy ($\sigma/L = 0.04$ m); (ii) Phase IV: focal seizures ($\sigma/L = 0.053$ m); (iii) Phase II: generalized seizures ($\sigma/L = 0.067$ m), with their steady states and corresponding eigenvalue spectra shown in Figs. 10(c)–10(h).

First, for the suppressed epilepsy, Fig. 10(c) shows consistency between the analytic solution and the numeric simulation of the stable steady state, with its stability indicated in Fig. 10(d). Their excellent match verifies the assumption of radial symmetry, and lends confidence in further analysis.

Second, for the focal seizures with larger σ/L, the steady state becomes unstable with mismatch between the analytic solution and the numeric simulation for the focal region, as shown in Fig. 10(e). Its instability is indicated by one eigenvalue having a positive real part [the rightmost blue star in Fig. 10(f)]. Here, the focal epilepsy is not suppressed but spatially limited without spreading over the whole system because σ/L is only large enough to resist suppression by the normal region. So the steady state is stable at the tail but unstable in the focal region.

Finally, for the generalized seizures with σ/L further increased, the steady state at the tail becomes unstable as well, and a ∼3-Hz wave originating from the focal region propagates over the whole system. One can find from Fig. 10(h) that there is one more eigenvalue along the bottom branch crossing the imaginary axis. Nonetheless, Fig. 10(g) shows the consistency between the time-averaged activity and the unstable steady state, suggesting that the activity at each spatial point surrounds the unstable steady state, and the ∼3-Hz wave emerges via a supercritical Hopf bifurcation.

The dynamical pictures for the above three scenarios are consistent with those indicated in eigenvalue spectra. Notice that Figs. 10(d), 10(f) and 10(h) show that most eigenvalues (red stars) align with two branches (black lines), where $L_{\mathrm{CT}}^{-1}(\lambda, \infty)$ is real and negative [$L_{\mathrm{CT}}^{-1}(\lambda, \infty) = 0$ at the branch right end]. These two branches correspond to resonances in the two delayed feedback loops: $e \to r \to s \to e$ and $e \to s \to e$, respectively, as in the spatially homogeneous case [30,44]. It is a general property in the delayed system that an infinite number of eigenvalues will align with such branches.

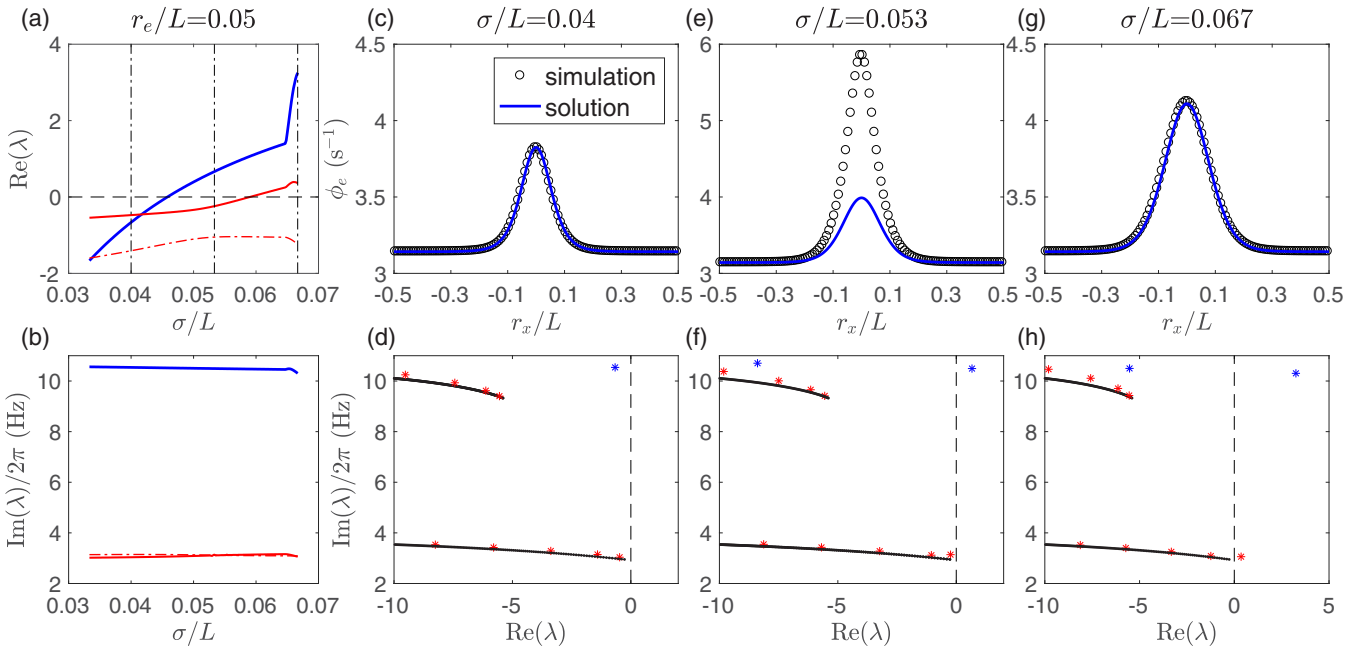

FIG. 10. Steady states and corresponding eigenvalue spectra. (a) Re(λ) vs σ/L at $r_e/L = 0.05$ for the three eigenvalues λ with largest Re(λ). Three vertical dash-dotted black lines indicate the values of σ/L for further analysis in (c)–(h). (b) Corresponding Im(λ) vs σ/L as in (a). (c) Stable steady state at $\sigma/L = 0.04$; (c) corresponding rightmost eigenvalues with largest Re(λ) (stars) at $\sigma/L = 0.04$. (e) Unstable steady state evolves to a localized ∼10-Hz wave at $\sigma/L = 0.053$; (f) corresponding rightmost eigenvalues with largest Re(λ) (stars) at $\sigma/L = 0.053$. (g) Unstable steady state evolves to a ∼3-Hz wave at $\sigma/L = 0.067$; (h) corresponding rightmost eigenvalues with largest Re(λ) (stars) at $\sigma/L = 0.067$. In (c), (e), and (g), steady states are compared between the time-averaged 1D spatial profile from simulations and the numerical solutions obtained from integration of Eq. (10);

Generally, the delay leads the spectrum of the system to be determined by the solutions of

$$W(\lambda)\exp[W(\lambda)] = \lambda, \tag{22}$$

where $W(\lambda)$ is a complex function with an infinite number of solutions [68]. It is continuous in the leftward spectrum with Re(λ) converging to negative infinity, while it becomes discrete in the rightward spectrum with Re(λ) getting close to zero. More mathematical details can be found in Ref. [68]. So most dynamical eigenmodes along the two branches correspond to resonances of the same corticothalamic loops as in the spatially homogeneous case.

However, some eigenvalues [blue stars in Figs. 10(d), 10(f) and 10(h)] emerge beyond these two branches, implying that their eigenmodes are not purely induced by the resonance of the underlying corticothalamic loops. For these eigenmodes, $L_{\mathrm{CT}}^{-1}(\lambda, \infty)$ has a much larger value than those with eigenvalues (red stars) close to the two branches. That means the steady state at the tail stays stable and far away from a corticothalamic loop resonance, while the system's steady state is unstable, as indicated in Fig. 10(f) with a positive Re(λ). Thus, such an eigenmode is confined to the focal region, as confirmed in Figs. 11(a) and 11(b). As a result, a different spatiotemporal wave with different frequency and waveform emerges from those of generalized seizures. What is more, the oscillation amplitude at each spatial point of such an eigenmode is also confined by its steady state's activity level, as shown in Fig. 11(b). This is in contrast with the eigenmode of generalized seizures, as shown in Figs. 11(c) and 11(d), where the wave propagates outward from the focal area, and the oscillation at each spatial point surrounds its steady state's activity level.

The localized ∼10-Hz waves are spatially limited due to the spatial confinement of the intrinsic steady state's activity levels. It also explains why edge effects destroy the pattern formation conditions for the focal seizures when there is not enough space to confine the waves away from the boundary. Furthermore, the spatially confined eigenmode in Figs. 11(a) and 11(b) is also unstable and then further evolves to another localized ∼10-Hz wave with a much higher amplitude, as seen in Fig. 10(e). So the focal seizures emerge suddenly from the suppressed instability via a subcritical Hopf bifurcation.

B. The role of corticothalamic loop

As shown in Figs. 10(d), 10(f) and 10(h), the emergence of the localized wave is different from the corticothalamic loop resonance in the homogeneous system. But they do not indicate that the emergence is independent on the underlying corticothalamic loop. To this end, we are employing the above eigenvalue spectra to investigate how alteration of the time lag t_d between cortex and thalamus affects the frequency of the spatially localized wave. As shown in Fig. 12, the frequency $f = \mathrm{Im}(\lambda)/2\pi$ is inversely dependent on t_d, which can be fitted as $f \approx 2\pi/(0.0086t_d + 0.25)$. This means the period T is linearly dependent on the time lag t_d, and thus the underlying corticothalamic loop has a significant contribution to the frequency of the emerged wave. Although this dependence is similar to that of the corticothalamic loop resonance in the

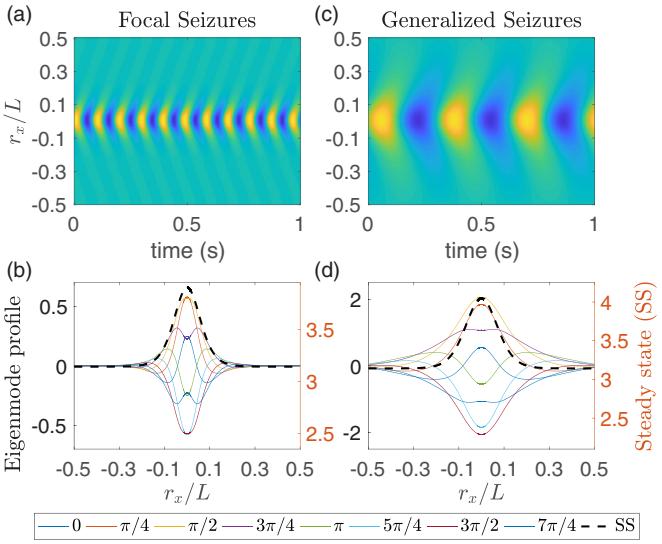

FIG. 11. Spatiotemporal eigenmodes of ∼10-Hz wave and ∼3-Hz wave at the respective critical points for $r_e/L = 0.05$. (a) One-dimensional wave dynamics of ϕ_e for points at $r_y = 0$ with $\sigma/L = 0.046$ for the focal seizures. (b) One-dimensional spatial profile of ϕ_e with $\sigma/L = 0.046$ for both eigenmodes and the corresponding steady states at $r_y = 0$ and various instantaneous phases φ_0, as indicated in the bottom legend. (c) Same as in (a) but with $\sigma/L = 0.059$ for the generalized seizures. (d) Same as in (b) but with $\sigma/L = 0.059$.

homogeneous system, the emergence of the localized wave does not require the resonance of the underlying corticothalamic loop. Thus, the localized wave is a spatiotemporal emergence with the contributions of both spatial confinement as well as the underlying corticothalamic loop.

C. Robustness of dynamical mechanism

The above dynamical mechanism for focal seizures is robust and does not require parameter fine-tuning. A large parameter region can be found in Figs. 13(a) and 13(b) where

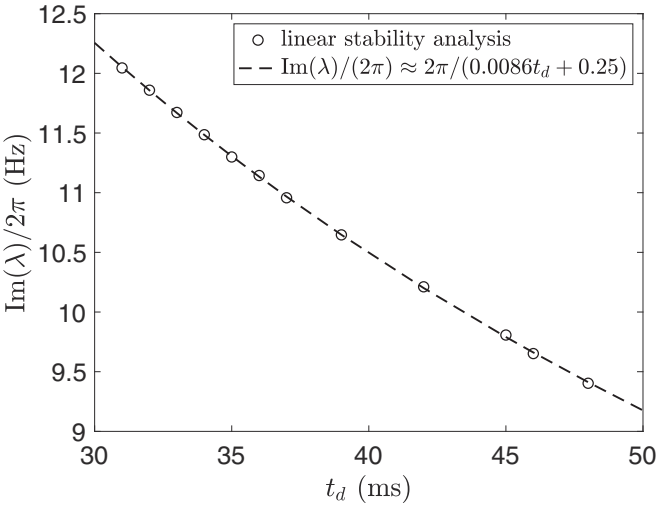

FIG. 12. Dependence of the frequency of the spatially localized wave on the time lag t_d between cortex and thalamus.

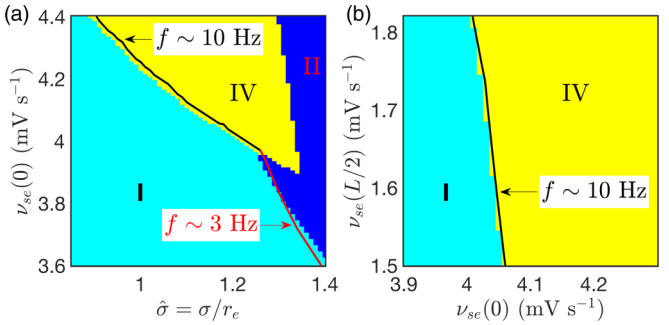

FIG. 13. Focal seizures due to strong nonlinear effects in the focus. (a) Phase diagram on $[\hat{\sigma}, \nu_{se}(0)]$; (b) phase diagram on $[\nu_{se}(0), \nu_{se}(L/2)]$ with $\hat{\sigma} = 1.2$. $\nu_{se}(L/2)$ has a much weaker effect on the emergence of focal seizures, in consistent with its underlying dynamical mechanism. The linear instability boundaries are also well predicted by linear stability analysis.

the focal activity is too unstable to be suppressed by the normal region, but does not generalize over the whole system, with $\nu_{se}(0)$ much larger than the linear stability boundary of the corticothalamic loops [the critical value $\nu_{se}^c \approx 1.98$ mV s, as indicated in Fig. 3(a) and Fig. 4(a)]. Figure 13(a) also shows that the suppressed epilepsy can transition directly to the generalized seizures when $\nu_{se}(0)$ is not large enough to induce the formation of focal seizures. This is the weakly nonlinear case explored in Ref. [69]. So the focal seizures emerge due to the combination of the spatial confinement, the underlying corticothalamic loop, as well as strong nonlinear effects of the focal area.

The above emergence also requires the normal region to be stable enough to be unevoked by the focal epilepsy. However, Fig. 13(b) shows that $\nu_{se}(L/2)$ has a much weaker effect. This is consistent with the underlying dynamical mechanism: for the focal seizures, the normal region is already stable and can resist invasion of seizure activity of the focus, so further lowering $\nu_{se}(L/2)$ to render the normal region more stable will make little contribution, as long as $\nu_{se}(0)$ is large enough to free the focal region from being suppressed by the normal region. These results are also consistent with the experimental findings in WAG/Rij and GAERS rats: pharmacological deactivation by blocking the neural activity of the driving cortical source can almost completely abolish SWDs in all cortical regions [17], while such deactivation in other cortical regions has little effect [70].

The simulation results are also confirmed by linear stability analysis, as shown in Fig. 13, indicating that the dynamical mechanism does not require some specific parameter. The dynamical mechanism can exist whenever the corticothalamic system has strong nonlinear effects in the focal area and the conditions for spatial confinement are satisfied.

V. SUMMARY AND DISCUSSION

This work has investigated how focal epilepsy can be suppressed, spatially limited, or generalized over the whole brain, via a physiology-based corticothalamic model with focal spatial heterogeneity. We found that the interplay between cortical propagation and the underlying corticothalamic

circuit can generate various spatiotemporal dynamics, dependent on the focal width σ and the axon range r_e scaled by the system size L. The main results are:

(i) The spatiotemporal dynamics summarized in the phase diagram (Fig. 5) have 6 phases, which can be categorized into three scenarios: suppressed epilepsy (Phase I and V), focal seizures (Phases IV, V, and VI), and generalized seizures (Phases II, III, and VI).

(ii) Axonal projections from the normal region can suppress the focal epilepsy when $\sigma/r_e \leqslant \hat{\sigma}_c$, whose value is mainly determined by the pathological value $\nu_{se}(0)$ of focal corticothalamic connection strength in this study.

(iii) In the generalized seizures, ∼3-Hz focal activity propagates rapidly over the whole system, with the temporal frequency and the spatial extent comparable with absence seizure activity in humans, and can be associated with the global aspect of absence epilepsy. Besides, the direction of propagating wave fronts can be reversed from outward to inward if r_e/L is small.

(iv) In the focal seizures, the spatially limited ∼10-Hz activity emerges due to strong nonlinear effects in the focal region and spatial confinement by the surrounding stable normal region, with the temporal frequency and the spatial extent comparable with absence seizure activity in genetic rat models, which can be associated with the focal aspect of absence epilepsy. This also provides a biophysical explanation of spatially more localized waves with higher oscillation frequency observed in rodents. Besides, the emergence can exist in the system with large-enough length to avoid edge effects, and thus general for other boundary conditions and cortical geometries.

(v) In both focal seizures and generalized seizures, the oscillation frequencies are robust, independent on r_e/L and σ/L, and the phase velocity v_p of the waves is much larger than the axon propagation speed.

(vi) In the focal seizures, v_p is predicted to depend linearly on the spatial extent w, which can be tested in experiments.

(vii) The underlying dynamical mechanisms for both focal seizures and generalized seizures are explained in detail through eigenvalue spectra and corresponding eigenmodes at critical states.

(viii) The stability in the normal region has a weaker effect on suppressing the focal epilepsy than the instability in the focal region. This result is consistent with the experimental findings of the effects of pharmacological deactivation on different cortical regions in WAG/Rij and GAERS rats [17,70]: Pharmacological deactivation by blocking the neural activity of the driving cortical source can almost completely abolish SWDs in all cortical regions [17], whereas such deactivation in other cortical regions has little effect [70].

Our results also have several implications for both theoretical and experimental further studies:

(i) The 7- to 11-Hz activity in WAG/Rij and GAERS rats may be explained by a relatively short axon length r_e/L, while r_e/L in human brains may be large enough to place the system in the regime dominated by edge effects, therefore inducing generalized seizures that spread over the whole system.

(ii) The spatially limited waves in the focal seizures can be modulated by ∼2-Hz slow waves. It is worth further investigating the underlying biophysical mechanism for such robust modulation in future.

(iii) In a narrow parameter range, the system can have two stable states: focal seizures and generalized seizures, referred to as Phase VI in Figs. 5 and 7. This phenomenon may explain the on-off intermittency of SWDs durations of absence seizures in the EEG of WAG/Rij rats [71], which also has chaotic properties.

In this work, we have focused on the interplay between cortical propagation and the underlying corticothalamic loop, which goes beyond most previous work on spatially extended heterogeneous but purely cortical models [72–75]. The emergence of the breathers was explored in previous work, but only in an abstract neural field model with Mexican hat connection profile and feedbacks, such as spike-frequency adaptation [58,76,77]. In most previous theoretical work, the sigmoid function was simplified to a step function, easing linear stability analysis [55,78]; however, the step function is unrealistic, whereas our corticothalamic model is physiologically justifiable, and relies on parameters that are experimentally measurable. Thus our results can be related back to the underlying physiological effects.

This work presents dynamical mechanisms for understanding how the characteristic range of corticocortical axons contributes to the interactions between normal arousal states and focal absence epilepsy and how the spatial extent of the focal seizure can account for the observed faster oscillations. The dynamical mechanism also provides a biophysical explanation of the temporally higher frequency, but spatially more localized, cortical waves observed in rodents. The key finding is the emergence of a different spectral peak from the macroscopic spatiotemporal interactions between normal states and seizure activities due to the underlying loop resonances. Such emergence is not connected to the time scales of microscopic cellular mechanisms. Hence, the spatiotemporal interactions are essential for understanding focal seizures and our work here provides a unified dynamical framework for both global and focal aspects of absence epilepsy.

This dynamical mechanism is different from the corticothalamic loop resonance in the spatially homogeneous case [30,31,44], which can be attributed to some specific underlying pathways, such as $e \to r \to s \to e$. However, here, the localized wave with a new oscillating frequency is an emergence phenomenon, due to the combination of spatial confinement, strong nonlinear effects in the focal area as well as the underlying corticothalamic loop. These effects are beyond that of the homogeneous system. At present, it is hard to say what kind of underlying pathways can lead the system to produce a localized wave with a new frequency. In our future work, more work should be conducted to explore the potential underlying pathways of the corticothalamic system for the emergence.

Additionally, our analysis of eigenvalue spectra and the corresponding eigenmodes uncovers the underlying dynamical mechanism of the emergence. The eigenmode for focal seizures provides a new perspective for analyzing the real data, e.g., ECoG and MEG signals on human patients, and initiates some further questions about the interplay of microscopic and macroscopic mechanisms for seizure activities, especially in absence seizures; for example: whether the

macroscopic brain dynamics is enough to describe seizure activities; what more biophysical properties are required, e.g., neuronal bursting; what is the interplay between microscopic and macroscopic mechanisms; whether the real data of absence seizures reflect the newly discovered spatiotemporal eigenmodes: temporally faster but spatially localized waves; what is the contribution of the macroscopic mechanisms in the observed data; and whether the eigenmodes can be used to track the macroscopic brain states for seizure prediction. We are currently seeking experimental data to validate our results and predictions, as well as to apply our newly discovered spatiotemporal patterns in real data analysis.

Some extensions could be investigated in future to account for more features of absence seizure activities:

(i) Thalamic relay neurons have well-characterized dual firing modes: bursting and tonic spiking. It was found recently in experiments that the rhythmic synchronized phasic firing of thalamic relay neuronal population can initiate SWDs and seems necessary for absence seizure maintenance [19]. The origin of such synchronization is shown from cortical drive and temporally framing via feedforward inhibition from cortical neurons to reticular neurons and then to relay neurons [20]. So it is essential to study the effect of neuronal firing modes and its interaction with the corticothalamic loop to bridge the gap between microscale mechanisms and macroscopic cortico-thalamo-cortical oscillations in absence epilepsy.

(ii) The specific somatosensory-thalamo-cortical network should be considered to further study the dynamical mechanism for SWD initiation, maintenance, and termination in genetic rat models [18,79]. The exact interactions between cortex and different thalamic nuclei are essential for understanding how the cortical 'focus' within the perioral subregion of the somatosensory cortex drives other parts of the cortex and the ventral basal complex of the thalamus.

(iii) SWDs are also affected by lesions and pharmacological manipulations of the basal ganglia (BG) and neuromodulator pathways [80,81]. The effect of BG has been proposed to be important for maintaining absence seizures over several tens of seconds by the dynamical loop of the BG-thalamocortical network [82], which also provides a modulation site and an intervention pathway to prevent absence seizures [83,84]. So it is essential to investigate the effect of BG modulation of focal epilepsy.

(iv) The transitions from the suppressed epilepsy to the focal seizures or the generalized seizures can be more systematically studied by employing normal form theory [44]. However, their canonical nature in the sense of normal form theory has not yet been rigorously justified for spatiotemporal evolution equations. But with some special perturbation modes, it can still be employed to understand the effects on bifurcation types of other biophysical properties, such as bursting activities in thalamic populations [5], the slow dynamics of extracellular potassium ion concentration [33], and spike frequency adaptation [85].

(v) Recently, the combination of homogeneous and heterogeneous spatial connectivity kernels has been proposed to be critical for synchronous seizure termination, which is a commonly observed phenomenon during seizures [86,87]. So it would be significant to extend our corticothalamic model with heterogeneous long-range spatial connectivity to study spatiotemporal dynamics of seizure activities.

ACKNOWLEDGMENTS

This work was supported by the Australian Research Council Center for Integrative Brain Function (Grant No. CE140100007) and by Australian Research Council Laureate Fellowship Grant No. FL140100025.

APPENDIX: DERIVATION OF $L_{\mathrm{CT}}(\lambda, r)$

Here we present the derivation of the radially symmetric linear operator $L_{\mathrm{CT}}(\lambda, r)$ for each spatial point of the corticothalamic system and each eigenmode corresponding to eigenvalue λ. The eigenvalue $\lambda = 0$ is for the stationary solution in Eqs. (10) and (12) and others for general eigenmodes in Eqs. (18) and (20).

We derive $L_{\mathrm{CT}}(\lambda, r)$ for both cases by imposing a small perturbation on either $[\phi_e^0(L/2), V_e^0(L/2), V_r^0(L/2), V_s^0(L/2)]$ or $[\phi_e^0(r), V_e^0(r), V_r^0(r), V_s^0(r)]$. Here the general perturbation with eigenvalue λ at position r is denoted as $[\hat{\phi}_e, \hat{V}_e, \hat{V}_r, \hat{V}_s]$, where the arguments (λ, r) are omitted for simplicity, which yields

$$[D(\lambda) - \mathscr{L}]\hat{\phi}_e = \hat{Q}_e, \tag{A1}$$

$$\hat{V}_e = L(\lambda)[\nu_{ee}\hat{\phi}_e + \nu_{ei}\hat{Q}_e + \nu_{es}\hat{Q}_s E(\lambda)], \tag{A2}$$

$$\hat{V}_r = L(\lambda)[\nu_{re}\hat{\phi}_e E(\lambda) + \nu_{rs}\hat{Q}_s], \tag{A3}$$

$$\hat{V}_s = L(\lambda)[\nu_{se}(r)\hat{\phi}_e E(\lambda) + \nu_{sr}\hat{Q}_r], \tag{A4}$$

with

$$E(\lambda) = \exp(-\lambda t_d), \tag{A5}$$

$$D(\lambda) = (1 + \lambda/\gamma_e)^2, \tag{A6}$$

$$L(\lambda) = (1 + \lambda/\alpha)^{-1}(1 + \lambda/\beta)^{-1}. \tag{A7}$$

By linearizing the sigmoid function near the steady state, Eqs (A2)–(A4) yield

$$\hat{Q}_e = [x + y_s z_s]\hat{\phi}_e, \tag{A8}$$

with

$$x = \frac{J_{ee}}{1 - J_{ei}}, \tag{A9}$$

$$y_s = \frac{J_{es}}{1 - J_{ei}}, \tag{A10}$$

$$z_s = \frac{J_{se} + J_{sre}}{1 - J_{srs}}, \tag{A11}$$

where $J_{abc} = J_{ab}J_{bc}$, and $J_{ab}(\lambda, r) = G_{ab}(r)L(\lambda)$ for connections within cortex or thalamus, and $J_{ab}(\lambda, r) = G_{ab}(r)L(\lambda)E(\lambda)$ for connections between cortex and thalamus with time delay t_d. Here x, y_s, and z_s are transfer functions for the signal propagating along axons from cortex to cortex, from thalamic relay nucleus to cortex, and from cortex to thalamic relay nucleus, respectively, as shown in Fig. 2 of Ref. [44]. The gain $G_{ab}(r) = \nu_{ab}\eta_a(r)Q_{\max}/\sigma'$ is the additional output

produced by neurons a per unit additional input from neurons b. Using Eqs (A1)–(A11), $L_{\rm CT}(\lambda, r)$ can be expressed as

$$L_{\rm CT}^{-1}(\lambda, r) = D(\lambda) - x(\lambda, r) - y_s(\lambda, r)z_s(\lambda, r), \qquad \text{(A12)}$$

which at $L_{\rm CT}^{-1}(\lambda, r) = 0$ yields the resonance of the corticothalamic loop for each radial distance r and each eigenmode with eigenvalue λ.

[1] V. Crunelli and N. Leresche, Childhood absence epilepsy: Genes, channels, neurons and networks, Nat. Rev. Neurosci. **3**, 371 (2002).

[2] H. K. M. Meeren, G. van Luijtelaar, F. H. Lopes da Silva, and A. M. L. Coenen, Evolving concepts on the pathophysiology of absence seizures: The cortical focus theory, Arch. Neurol. **62**, 371 (2005).

[3] A. Depaulis and S. Charpier, Pathophysiology of absence epilepsy: Insights from genetic models, Neurosci. Lett. **667**, 53 (2018).

[4] R. S. Fisher and D. A. Prince, Spike-wave rhythms in cat cortex induced by parenteral penicillin. I. Electroencephalographic features, Electroencephalogr. Clin. Neurophysiol. **42**, 608 (1977).

[5] A. Destexhe, Spike-and-wave oscillations based on the properties of $GABA_B$ receptors, J. Neurosci. **18**, 9099 (1998).

[6] F. H. Lopes da Silva, W. Blanes, S. N. Kalitzin, J. Parra, P. Suffczynski, and D. N. Velis, Epilepsies as dynamical diseases of brain systems: Basic models of the transition between normal and epileptic activity, Epilepsia **44**, 72 (2003).

[7] H. K. Meeren, J. G. Veening, T. A. Möderscheim, A. M. Coenen, and G. van Luijtelaar, Thalamic lesions in a genetic rat model of absence epilepsy: Dissociation between spike-wave discharges and sleep spindles, Exp. Neurol. **217**, 25 (2009).

[8] M. Avoli, A brief history on the oscillating roles of thalamus and cortex in absence seizures, Epilepsia **53**, 779 (2012).

[9] H. K. M. Meeren, J. P. M. Pijn, E. L. J. M. van Luijtelaar, A. M. L. Coenen, and F. H. Lopes da Silva, Cortical focus drives widespread corticothalamic networks during spontaneous absence seizures in rats, J. Neurosci. **22**, 1480 (2002).

[10] E. Sitnikova and G. van Luijtelaar, Cortical control of generalized absence seizures: effect of lidocaine applied to the somatosensory cortex in WAG/Rij rats, Brain Res. **1012**, 127 (2004).

[11] P.-O. Polack, I. Guillemain, E. Hu, C. Deransart, A. Depaulis, and S. Charpier, Deep layer somatosensory cortical neurons initiate spike-and-wave discharges in a genetic model of absence seizures, J. Neurosci. **27**, 6590 (2007).

[12] P.-O. Polack, S. Mahon, M. Chavez, and S. Charpier, Inactivation of the somatosensory cortex prevents paroxysmal oscillations in cortical and related thalamic neurons in a genetic model of absence epilepsy, Cereb. Cortex **19**, 2078 (2009).

[13] F. Scicchitano, C. M. van Rijn, and G. van Luijtelaar, Unilateral and bilateral cortical resection: Effects on spike-wave discharges in a genetic absence epilepsy model, PLOS ONE **10**, e0133594 (2015).

[14] M. D. Holmes, M. Brown, and D. M. Tucker, Are "generalize" seizures truly generalized? Evidence of localized mesial frontal and frontopolar discharges in absence, Epilepsia **45**, 1568 (2004).

[15] P. G. Sarrigiannis, Y. Zhao, F. He, S. A. Billings, K. Baster, C. Rittey, J. Yianni, P. Zis, H. Wei, M. Hadjivassiliou, and R. Grünewald, The cortical focus in childhood absence epilepsy; evidence from nonlinear analysis of scalp EEG recordings, Clin. Neurophysiol. **129**, 602 (2018).

[16] H. Blumenfeld, Cellular and network mechanisms of spike-wave seizures, Epilepsia **46**, 21 (2005).

[17] G. van Luijtelaar and E. Sitnikova, Global and focal aspects of absence epilepsy: The contribution of genetic models, Neurosci. Biobehav. Rev. **30**, 983 (2006).

[18] A. Lüttjohann and G. van Luijtelaar, Dynamics of networks during absence seizure's on- and offset in rodents and man, Front. Physiol. **6**, 16 (2015).

[19] J. M. Sorokin, T. J. Davidson, E. Frechette, A. M. Abramian, K. Deisseroth, J. R. Huguenard, and J. T. Paz, Bidirectional control of generalized epilepsy networks via rapid real-time switching of firing mode, Neuron **93**, 194 (2017).

[20] C. McCafferty, F. David, M. Venzi, M. L. Lőrincz, F. Delicata, Z. Atherton, G. Recchia, G. Orban, R. C. Lambert, G. Di Giovanni, N. Leresche, and V. Crunelli, Cortical drive and thalamic feed-forward inhibition control thalamic output synchrony during absence seizures, Nat. Neurosci. **21**, 744 (2018).

[21] E. Bullmore and O. Sporns, Complex brain networks: Graph theoretical analysis of structural and functional systems, Nat. Rev. Neurosci. **10**, 186 (2009).

[22] O. Sporns, Structure and function of complex brain networks, Dialogues Clin. Neurosci. **15**, 247 (2013).

[23] M. Breakspear, Dynamic models of large-scale brain activity, Nat. Neurosci. **20**, 340 (2017).

[24] S. M. Sherman, Thalamus plays a central role in ongoing cortical functioning, Nat. Neurosci. **19**, 533 (2016).

[25] G. Deco, V. Jirsa, A. R. McIntosh, O. Sporns, and R. Kotter, Key role of coupling, delay, and noise in resting brain fluctuations, Proc. Nat. Acad. Sci. USA **106**, 10302 (2009).

[26] *Neocortical Dynamics and Human EEG Rhythms*, edited by P. L. Nunez and B. A. Cutillo (Oxford University Press, New York, 1995).

[27] V. K. Jirsa and H. Haken, Field Theory of Electromagnetic Brain Activity, Phys. Rev. Lett. **77**, 960 (1996).

[28] P. A. Robinson, C. J. Rennie, and J. J. Wright, Propagation and stability of waves of electrical activity in the cerebral cortex, Phys. Rev. E **56**, 826 (1997).

[29] G. Deco, V. K. Jirsa, P. A. Robinson, M. Breakspear, and K. Friston, The dynamic brain: From spiking neurons to neural masses and cortical fields, PLoS Comput. Biol. **4**, e1000092 (2008).

[30] P. A. Robinson, C. J. Rennie, and D. L. Rowe, Dynamics of large-scale brain activity in normal arousal states and epileptic seizures, Phys. Rev. E **65**, 041924 (2002).

[31] M. Breakspear, J. A. Roberts, J. R. Terry, S. Rodrigues, N. Mahant, and P. A. Robinson, A unifying explanation of primary generalized seizures through nonlinear brain modeling and bifurcation analysis, Cereb. Cortex **16**, 1296 (2006).

[32] D. A. McCormick and D. Contreras, On the cellular and network bases of epileptic seizures, Annu. Rev. Physiol. **63**, 815 (2001).

[33] M. Bazhenov, I. Timofeev, F. Fröhlich, and T. J. Sejnowski, Cellular and network mechanisms of electrographic seizures, Drug Discov Today Dis. Models **5**, 45 (2008).

[34] A. M. L. Coenen and E. L. J. M. van Luijtelaar, Genetic animal models for absence epilepsy: A review of the WAG/Rij strain of rats, Behav. Genet. **33**, 635 (2003).

[35] D. Pinault and T. J. O'brien, Cellular and network mechanisms of genetically-determined absence seizures, Thalamus Rel. Syst. **3**, 181 (2005).

[36] A. Destexhe, Can $GABA_A$ conductances explain the fast oscillation frequency of absence seizures in rodents? Eur. J. Neurosci. **11**, 2175 (1999).

[37] A. Destexhe, Network models of absence seizures, in *Neuronal Networks in Brain Function, CNS Disorders, and Therapeutics*, edited by C. L. Faingold and H. Blumenfeld (Elsevier, San Diego, CA, 2014), pp. 11–35.

[38] H. Nersesyan, F. Hyder, D. L. Rothman, and H. Blumenfeld, Dynamic fMRI and EEG recordings during spike-wave seizures and generalized tonic-clonic seizures in WAG/Rij tats, J. Cereb. Blood Flow Metab. **24**, 589 (2004).

[39] F. H. Lopes da Silva, A. van Rotterdam, W. S. van Leeuwen, and A. Tielen, Dynamic characteristics of visual evoked potentials in the dog. II. Beta frequency selectivity in evoked potentials and background activity, Electroencephalogr. Clin. Neurophysiol. **29**, 260 (1970).

[40] P. A. Robinson, Neurophysical theory of coherence and correlations of electroencephalographic and electrocorticographic signals, J. Theor. Biol. **222**, 163 (2003).

[41] V. Braitenberg and A. Schüz, *Cortex: Statistics and Geometry of Neuronal Connectivity* (Springer Science & Business Media, New York, 2013).

[42] D. T. J. Liley and J. J. Wright, Intracortical connectivity of pyramidal and stellate cells: Estimates of synaptic densities and coupling symmetry, Netw. Comput. Neur. Syst. **5**, 175 (1994).

[43] J. J. Wright and D. T. J. Liley, Dynamics of the brain at global and microscopic scales: Neural networks and the eeg, Behav. Brain Sci. **19**, 285 (1996).

[44] D.-P. Yang and P. A. Robinson, Critical dynamics of hopf bifurcations in the corticothalamic system: Transitions from normal arousal states to epileptic seizures, Phys. Rev. E **95**, 042410 (2017).

[45] A. Destexhe and T. J. Sejnowski, *Thalamocortical Assemblies* (Oxford University Press, Oxford, 2001).

[46] P. Sanz-Leon, P. A. Robinson, S. A. Knock, P. M. Drysdale, R. G. Abeysuriya, F. K. Fung, C. J. Rennie, and X. Zhao, NFTsim: Theory and simulation of multiscale neural field dynamics, PLoS Comput. Biol. **14**, e1006387 (2018).

[47] R. Courant, K. Friedrichs, and H. Lewy, On the partial difference equations of mathematical physics, IBM J. Res. Dev. **11**, 215 (1967).

[48] W. J. Firth and A. J. Scroggie, Optical Bullet Holes: Robust Controllable Localized States of a Nonlinear Cavity, Phys. Rev. Lett. **76**, 1623 (1996).

[49] P. A. Robinson, C. J. Rennie, D. L. Rowe, S. C. O'Connor, and E. Gordon, Multiscale brain modelling, Philos. Trans. R. Soc. Lond. B Biol. Sci. **360**, 1043 (2005).

[50] P. A. Robinson, C. J. Rennie, J. J. Wright, and P. D. Bourke, Steady states and global dynamics of electrical activity in the cerebral cortex, Phys. Rev. E **58**, 3557 (1998).

[51] F. Freyer, J. A. Roberts, R. Becker, P. A. Robinson, P. Ritter, and M. Breakspear, Biophysical mechanisms of multistability in resting-state cortical rhythms, J. Neurosci. **31**, 6353 (2011).

[52] F. H. Lopes da Silva, W. Blanes, S. N. Kalitzin, J. Parra, P. Suffczynski, and D. N. Velis, Dynamical diseases of brain systems: Different routes to epileptic seizures, IEEE Trans. Biomed. Eng. **50**, 540 (2003).

[53] F. B. Neubauer, A. Sederberg, and J. N. MacLean, Local changes in neocortical circuit dynamics coincide with the spread of seizures to thalamus in a model of epilepsy, Front. Neur. Circ. **8**, 101 (2014).

[54] P. A. Robinson, C. J. Rennie, D. L. Rowe, and S. C. O'Connor, Estimation of multiscale neurophysiologic parameters by electroencephalographic means, Hum. Brain Map. **23**, 53 (2004).

[55] S. Coombes and M. R. Owen, Evans functions for integral neural field equations with heaviside firing rate function, SIAM J. Appl. Dyn. Syst. **3**, 574 (2004).

[56] D. J. Englot *et al.*, Impaired consciousness in temporal lobe seizures: Tole of cortical slow activity, Brain **133**, 3764 (2010).

[57] M. Rosanova, O. Gosseries, S. Casarotto, M. Boly, A. G. Casali, M.-A. Bruno, M. Mariotti, P. Boveroux, G. Tononi, S. Laureys, and M. Massimini, Recovery of cortical effective connectivity and recovery of consciousness in vegetative patients, Brain **135**, 1308 (2012).

[58] S. E. Folias and P. C. Bressloff, Breathers in Two-Dimensional Neural Media, Phys. Rev. Lett. **95**, 208107 (2005).

[59] S. E. Folias, Traveling waves and breathers in an excitatory-inhibitory neural field, Phys. Rev. E **95**, 032210 (2017).

[60] R. D. Chervin, P. A. Pierce, and B. W. Connors, Periodicity and directionality in the propagation of epileptiform discharges across neocortex, J. Neurophysiol. **60**, 1695 (1988).

[61] M. A. Kramer, H. E. Kirsch, and A. J. Szeri, Pathological pattern formation and cortical propagation of epileptic seizures, J. Royal Soc. Interface **2**, 113 (2005).

[62] D. J. Pinto, S. L. Patrick, W. C. Huang, and B. W. Connors, Initiation, propagation, and termination of epileptiform activity in rodent neocortex *in vitro* involve distinct mechanisms, J. Neurosci. **25**, 8131 (2005).

[63] A. J. Trevelyan, D. Sussillo, and R. Yuste, Feedforward inhibition contributes to the control of epileptiform propagation speed, J. Neurosci. **27**, 3383 (2007).

[64] L. Muller and A. Destexhe, Propagating waves in thalamus, cortex and the thalamocortical system: Experiments and models, J. Physiol. Paris **106**, 222 (2012).

[65] A. J. Trevelyan and C. A. Schevon, How inhibition influences seizure propagation, Neuropharmacol. **69**, 45 (2013).

[66] L.-E. Martinet, O. J. Ahmed, K. Q. Lepage, S. S. Cash, and M. A. Kramer, Slow spatial recruitment of neocortex during secondarily generalized seizures and its relation to surgical outcome, J. Neurosci. **35**, 9477 (2015).

[67] L.-E. Martinet, G. Fiddyment, J. R. Madsen, E. N. Eskandar, W. Truccolo, U. T. Eden, S. S. Cash, and M. A. Kramer, Human seizures couple across spatial scales through traveling wave dynamics, Nat. Commun. **8**, 14896 (2017).

[68] P. Grindrod and D. Pinotsis, On the spectra of certain integro-differential-delay problems with applications in neurodynamics, Physica D **240**, 13 (2011).

[69] J. W. Kim, J. A. Roberts, and P. A. Robinson, Dynamics of epileptic seizures: Evolution, spreading, and suppression, J. Theor. Biol. **257**, 527 (2009).

[70] G. van Luijtelaar, E. Sitnikova, and A. Luttjohann, On the origin and suddenness of absences in genetic absence models, Clin. EEG Neurosci. **42**, 83 (2011).

[71] E. Sitnikova, A. E. Hramov, V. V. Grubov, A. A. Ovchinnkov, and A. A. Koronovsky, On–off intermittency of thalamo-cortical oscillations in the electroencephalogram of rats with genetic predisposition to absence epilepsy, Brain Res. **1436**, 147 (2012).

[72] P. N. Taylor and G. Baier, A spatially extended model for macroscopic spike-wave discharges, J. Comput. Neurosci. **31**, 679 (2011).

[73] M. Goodfellow, K. Schindler, and G. Baier, Intermittent spike–wave dynamics in a heterogeneous, spatially extended neural mass model, NeuroImage **55**, 920 (2011).

[74] G. Marc, T. P. Neal, W. Yujiang, G. D. James, and B. Gerold, Modelling the role of tissue heterogeneity in epileptic rhythms, Eur. J. Neurosci. **36**, 2178 (2012).

[75] P. N. Taylor, M. Goodfellow, Y. Wang, and G. Baier, Towards a large-scale model of patient-specific epileptic spike-wave discharges, Biol. Cybern. **107**, 83 (2013).

[76] S. Coombes and M. R. Owen, Bumps, Breathers, and Waves in a Neural Network with Spike Frequency Adaptation, Phys. Rev. Lett. **94**, 148102 (2005).

[77] Y. Qi and P. Gong, Dynamic patterns in a two-dimensional neural field with refractoriness, Phys. Rev. E **92**, 022702 (2015).

[78] P. N. Loxley and P. A. Robinson, Soliton Model of Competitive Neural Dynamics During Binocular Rivalry, Phys. Rev. Lett. **102**, 258701 (2009).

[79] M. Sysoeva, A. Lüttjohann, G. van Luijtelaar, and I. Sysoev, Dynamics of directional coupling underlying spike-wave discharges, Neuroscience **314**, 75 (2016).

[80] L. Danober, A. Depaulis, C. Marescaux, and M. Vergnes, Effects of cholinergic drugs on genetic absence seizures in rats, Eur. J. Pharmacol. **234**, 263 (1993).

[81] L. Danober, C. Deransart, A. Depaulis, M. Vergnes, and C. Marescaux, Pathophysiological mechanisms of genetic absence epilepsy in the rat, Prog. Neurobiol. **55**, 27 (1998).

[82] T. Arakaki, S. Mahon, S. Charpier, A. Leblois, and D. Hansel, The role of striatal feedforward inhibition in the maintenance of absence seizures, J. Neurosci. **36**, 9618 (2016).

[83] M. Chen, D. Guo, T. Wang, W. Jing, Y. Xia, P. Xu, C. Luo, P. A. Valdes-Sosa, and D. Yao, Bidirectional control of absence seizures by the basal ganglia: A computational evidence, PLoS Comput. Biol. **10**, e1003495 (2014).

[84] M. Chen, D. Guo, M. Li, T. Ma, S. Wu, J. Ma, Y. Cui, Y. Xia, P. Xu, and D. Yao, Critical roles of the direct gabaergic pallido-cortical pathway in controlling absence seizures, PLoS Comput. Biol. **11**, e1004539 (2015).

[85] Y.-H. Liu and X.-J. Wang, Spike-frequency adaptation of a generalized leaky integrate-and-fire model neuron, J. Comput. Neurosci **10**, 25 (2001).

[86] W. Truccolo, J. A. Donoghue, L. R. Hochberg, E. N. Eskandar, J. R. Madsen, W. S. Anderson, E. N. Brown, E. Halgren, and S. S. Cash, Single-neuron dynamics in human focal epilepsy, Nat. Neurosci. **14**, 635 (2011).

[87] T. Proix, V. K. Jirsa, F. Bartolomei, M. Guye, and W. Truccolo, Predicting the spatiotemporal diversity of seizure propagation and termination in human focal epilepsy, Nat. Commun. **9**, 1088 (2018).